Behaviour of heated steel beams with lateral and axial restraint in steel-timber hybrid structures

Aatish Jeebodh[a,*], Buick Davison[a], Martyn S. McLaggan[a], Ian Burgess[a], Danny Hopkin[b], Shan-Shan Huang[a]

[a] University of Sheffield, Sheffield, S1 3JD, UK

[b] OFR Consultants, The Manse, 44 South Bar, Banbury, Oxford, OX16 9AB, UK

[*] Corresponding author. E-mail address: ajeebodh1@sheffield.ac.uk

Abstract

Amidst the climate emergency and ambitions to decarbonise the built environment, hybrid systems consisting of a steel structural frame supporting cross-laminated timber floors have emerged as a new paradigm in sustainable construction. While this form of hybridisation is beneficial in many ways, it also presents certain challenges, particularly regarding its structural performance in fire. A critical concern in fire is the risk of lateral-torsional buckling of the steel beams connected to the timber slabs with self-tapping screws, which goes beyond the scope of current design guidance. Using a numerical approach, this study has developed finite element modelling capacity to investigate the thermo-mechanical response of a 9 m unprotected steel beam with screws at 250 mm spacing under various levels of lateral restraint from the screws and axial restraint from the end connections. The imposed heating regimes have also explored the influence of the temperature on the compression flanges of the steel beam. When axial restraint is present, indicating a realistic support condition in fire, the beam initially behaves similarly to a corresponding fully laterally restrained beam. This response continues until the first screw fails in the midspan region, which eventually triggers instability by lateral-torsional buckling. The results highlight the significance of lateral restraint in enhancing the fire performance of steel-timber hybrid structures. However, it is not realistic to assume a full lateral restraint condition in fire design.

Keywords: Steel-timber hybrid structures; Lateral-torsional buckling; Fire; Parametric study; Thermo-mechanical modelling

1. Introduction

In recent years, steel-timber hybrid structures have emerged as a viable form of construction in response to the climate crisis and as demands for sustainability continue to escalate in the built environment. This hybrid approach to construction makes use of traditional steel frames integrated with cross-laminated timber (CLT) slabs, which are typically supported by the steel beams in downstand or slimfloor arrangements. In a downstand arrangement, the floor slab is supported on the top flanges of the beams, whereas the slimfloor arrangement makes it

possible to support the floor directly on the wide bottom flanges of bespoke asymmetric beams. Steel-timber hybrid solutions offer several key environmental, structural and fabrication benefits over the widely used and well-established steel-concrete hybrid structures. However, the adoption of combustible timber structural elements in hybrid systems is beyond the scope of structural design guidance currently available for the fire limit state, particularly for the lateral-torsional buckling behaviour of the steel beams in a downstand arrangement at elevated temperatures [1, 2]. Additionally, the occurrence of end axial restraint from the surrounding structure can fundamentally change the response of the beams in fire as the development of compressive axial forces due to restrained thermal expansion can further increase their susceptibility to lateral-torsional buckling [3]. This is particularly important during the initial stages of a fire, when the beam response is predominantly elastic, and before very large deflections start to occur.

Over the last few decades, structural fire engineering approaches have been established for steel framed structures with concrete slabs [4], and there is now an urgency to extend this knowledge and understanding to steel frames with CLT slabs. This is necessary to overcome the barriers faced by various construction stakeholders in adopting this relatively novel form of hybridisation, especially as the demand for this low-carbon topology continues to grow in the built environment as a response to the climate emergency. In conventional steel-concrete composite structures, the top flange of a downstand steel beam is normally assumed by designers to be fully restrained laterally under both ambient and fire conditions. In such cases, it is normally possible to achieve the full-in plane bending resistance of the beam. This may not be applicable to a steel-timber hybrid beam in fire, as lateral-torsional buckling instability may occur before the beam can attain its full moment capacity. Lateral restraint of the upper flange of the steel beam in steel-timber hybrid structures is traditionally achieved using closely-spaced self-tapping screws. Merryday et al. [5] conducted a four-point bending test on a simply supported steel-CLT composite beam with self-tapping screws and reported that lateral-torsional buckling is not a concern at ambient temperature, even with a narrow width of CLT slab. This finding from a bending test indicates that the screws offer an adequate degree of lateral stiffness to prevent beam lateral-torsional buckling at ambient temperature, but this must also be verified under fire conditions due to degradation of the connectors at elevated temperatures.

Hence, the aim of this study is to investigate the behaviour of unprotected downstand steel beams in steel-timber hybrid structures against lateral-torsional buckling and restrained thermal expansion in fire. The objectives are: (i) to assess the level of lateral restraint mobilised by self-tapping screws based on existing literature, and (ii) to develop finite element modelling capacity to effectively investigate the lateral-torsional buckling behaviour of heated steel beams with top flange lateral restraint and end axial restraint. It must be noted that in this study the timber slab is not explicitly modelled for mechanical response but the connection between the steel beam and the timber slab is accounted for through the lateral stiffness provided by the fixings. There is little to no guidance on the design of steel-timber

composite construction in current practice, so designers conservatively ignore any potential contribution of CLT panels to composite action and assume that the steel beams resist the full applied loading [1, 5, 6]. The composite action of steel-timber beams has been investigated under ambient temperature conditions. CLT panels with a greater number of longitudinal layers aligned with the beam span have been shown to contribute more significantly to bending stiffness [7]. However, the structural response of such systems under fire conditions remains largely unknown and represents an important area for future research. Therefore, this study deals with the case of steel beams without composite action with the timber slab, but the influence of the floor slab as a potential heat sink in the thermal response is considered. The assumptions made in this study with reference to the lateral restraints are conservative, and it is possible that partial composite action during a fire could result in higher flexural stiffness than that of a non-composite steel beam and a separate CLT slab; however, the extent of this effect is unknown.

2. Lateral restraint of self-tapping screws

This section provides an overview of the lateral stiffness characteristics of the self-tapping screws conventionally adopted in mass timber assemblies. Steel-timber hybrid structures can be designed with the connectors acting as lateral restraint to the top flange of the steel beam to prevent beam lateral-torsional buckling. In common practice, CLT panels are attached to steel beams using partially threaded or fully threaded self-tapping screws. The standard screw layout for steel-to-timber connections varies by project, but it is generally provided at spacings not exceeding 600 mm [1]. Staggering of the screws is also recommended to reduce the possibility of wood splitting during installation of the fasteners and potentially to avoid overlapping of thermally affected areas of the timber in the vicinity of the screws, which might as a consequence affect the lateral shear resistance and pull-out resistance of the connectors in fire.

The screws, when loaded in shear, provide a degree of lateral stiffness against lateral-torsional buckling of the steel beam. For design purposes, the lateral stiffness offered by screws is defined in terms of the slip modulus for different limit states: K_{ser} for the serviceability limit state, K_u for the ultimate limit state, and K_{fi} for the fire limit state. The slip modulus for the serviceability limit state K_{ser} can be determined experimentally by means of push-out tests or using semi-empirical expressions. K_u is taken as two-thirds of K_{ser} as per BS EN 1995-1-1:2004+A2 [8]. For fire design in accordance with BS EN 1995-1-2 [9], the slip modulus K_{fi} should be taken as 20% of K_u for screw connections and 67% of K_u for bolted connections. It must be noted that a single value of K_{fi} is adopted in fire and no consideration is given to the variation in connector properties at different temperatures. Figure 1 illustrates the procedure as set out in Eurocode 5 to determine the slip modulus of mechanical fasteners for different limit states. More detailed information on the lateral stiffness characteristics of steel-to-CLT connections using self-tapping screws can be found in Jeebodh et al. [10].

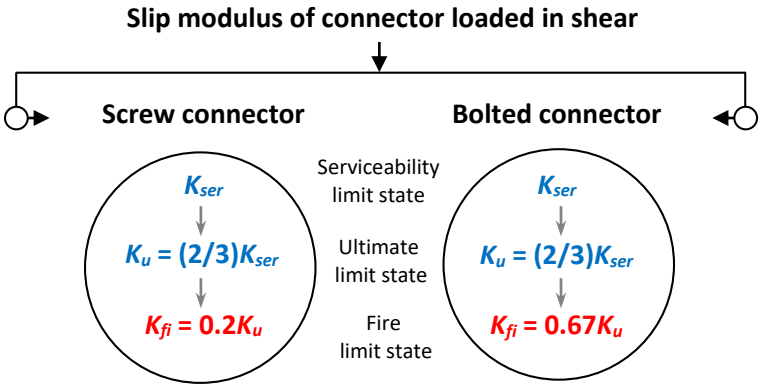

Figure 1: Flowchart for determination of slip modulus as per Eurocode 5 guidance

The load-slip relationship of steel-to-CLT connections using self-tapping screws is generally characterised by non-linear behaviour at ambient temperature. Experimental investigations to quantify the longitudinal shear capacity of the steel-timber connections with self-tapping screws in fire are lacking. Merryday et al. [6] conducted several monotonic push-out tests to study the response of steel-to-CLT connections assembled using three brands of self-tapping screws of different geometries (Type A, B and C) at ambient temperature. The screws were subjected to shear at the interface plane between the steel beam and the timber slab.

Figure 2 shows the average load-slip behaviour of three laterally-loaded screw connection specimens with similar screw length, screw spacing, and CLT orientation, but with each specimen connected using a different brand of self-tapping screw. The remaining push-out performance for other test configurations can be found in [6]. From the experimental results, it can be observed that the screws exhibited different stiffness, strength and ductility. The majority of Type A screws demonstrated ductile behaviour, while Type B and C screws showed more brittle behaviour. The load-slip results from the tests were used in this study to determine the serviceability slip modulus K_{ser} in accordance with BS EN 26891 [11] equations. The serviceability stiffness K_{ser} varies approximately between 1500 N/mm and 3500 N/mm per 12 mm nominal diameter screw. Hence, K_{fi} can be assumed to vary approximately between 200 N/mm and 467 N/mm for the tested screws at the fire limit state according to Eurocode 5 guidance. As expected, slightly lower levels of stiffness for 10 mm screws in steel-to-CLT connections have been observed by Asiz and Smith [12]. However, the present study focuses on large diameter (12 mm) self-tapping screws which are likely to be more suitable for large-scale construction, as fabrication of small-diameter holes through thicker steel members may be difficult for the steel fabricator [1, 2, 6] and also to harness the benefits of higher slip modulus per screw.

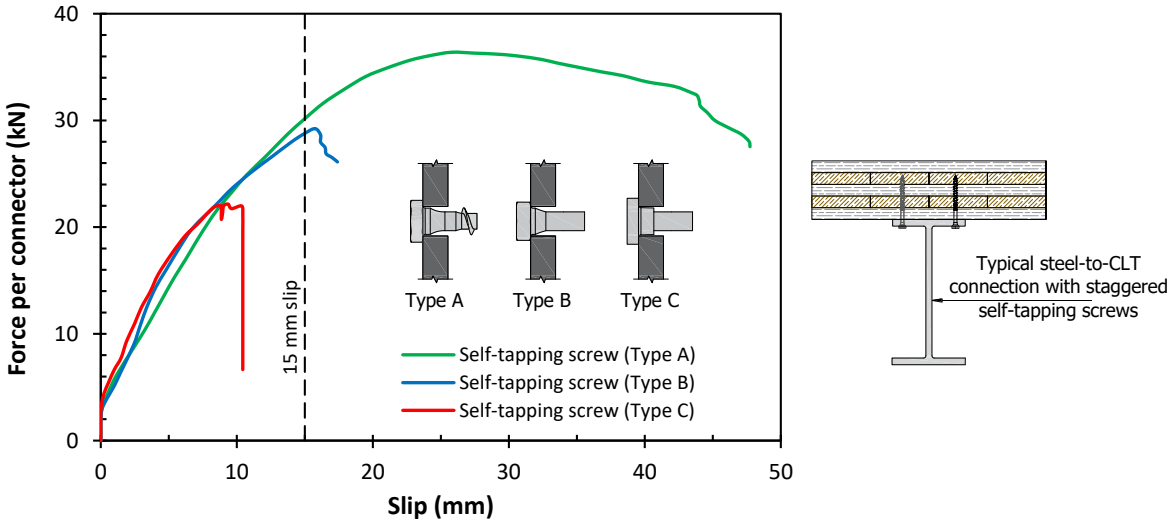

Figure 2: Average load-slip curves of push-out tests using three different screw brands [6]

3. Finite element modelling in fire

The structural fire behaviour of steel-timber hybrid structures is mainly influenced by design decisions such as the beam-slab typology, type of connection, choice of adhesive, fire type, and the adopted fire safety strategy. As such, a better comprehension of the thermo-mechanical behaviour of such systems via experimental and/or numerical studies is essential to develop structural fire engineering approaches, with the aim of determining the best practices to design and construct robust steel-timber hybrid structures to resist fire conditions. This section presents the development of finite element models: (i) to capture the thermal response of steel beams supporting a timber flooring system in fire by heat transfer analysis, and (ii) to replicate the lateral-torsional buckling behaviour in the presence of axial restraint of heated steel beams using high temperature mechanical analysis. The numerical models were developed using the finite element analysis software *Abaqus* [13] and validated against experimental results from literature.

3.1 Development and validation of heat transfer model

Knowledge of heat transfer is essential to understand the thermal response of hybrid structures in fire. Whether in a fire compartment or a laboratory furnace, heat energy is transferred by the mechanisms of conduction, convection and radiation. When the top flange of a steel beam is attached to a timber or concrete flooring system and is immersed in the flames and hot gases of a fire, both the steel section and bottom surface of the floor receive thermal energy by convection from the hot gases and radiation by electromagnetic waves from the flames. Radiation is key as it is generally the dominant mechanism of energy transfer in large fire situations and is crucial for accurate temperature prediction in numerical models [14]. In a downstand configuration, the beam is generally subjected to heating from three sides and as it begins to heat up, thermal energy is transferred through the steel material by

conduction and eventually deeper into the upper floor which is in direct contact with the top flange of the beam.

In accordance with Eurocode 1 [15], the thermal action on a surface exposed to fire can be represented by a net heat flux $\dot{h}_{net}$, which is defined by the sum of convective $\dot{h}_{net,c}$ and radiative $\dot{h}_{net,r}$ flows as given by:

$$\dot{h}_{net} = \dot{h}_{net,c} + \dot{h}_{net,r} \tag{1}$$

The net convective heat flux component is determined using the following equation:

$$\dot{h}_{net,c} = \alpha_c(\theta_g - \theta_m) \tag{2}$$

where α_c is the coefficient of heat transfer by convection, θ_g is the gas temperature, and θ_m is the surface temperature of the member. In a heat transfer model, the code recommends α_c is taken as 25 W/m²K on the fire-exposed surface to a standard fire and 9 W/m²K on the unexposed side.

The net radiative heat flux component per unit surface area is given by:

$$\dot{h}_{net,r} = \phi \cdot \varepsilon_m \cdot \varepsilon_f \cdot \sigma\left[(\theta_r + 273)^4 - (\theta_m + 273)^4\right] \tag{3}$$

Where ϕ is the configuration factor, ε_m is the surface emissivity of the material, ε_f is the emissivity of the fire, σ is the Stephan-Boltzmann constant (5.67×10^{-8} W/m²K⁴), θ_r is the radiation temperature of the fire environment taken as equal to θ_g in the case of members fully engulfed in fire, and θ_m is the surface temperature of the member. The configuration factor ϕ is normally taken as 1.0 but a lower value can be used to take into consideration the shadow effects. $\varepsilon_m = 0.7$ for the surface of steel and concrete and $\varepsilon_m = 0.8$ for the surface of timber. The emissivity of the fire is in general taken as $\varepsilon_f = 1.0$.

In numerical simulations, the thermal boundary conditions of the surfaces of members exposed to convection and radiation must be realistically represented to obtain accurate temperature distributions. In fully developed compartment fires, radiation is generally acknowledged as the dominant mode of the total heat flux [14] and due to the complexity in determining the correct heat transfer parameters for the radiation flux on individual surfaces, Equation (3) has been simplified [16] using an equivalent emissivity of $\in_{eq}$, which takes into account the shadow effects of the incident radiation and emissivities of the fire and the steel member.

$$\dot{h}_{net,r} = \in_{eq} \cdot\sigma\left[(\theta_r + 273)^4 - (\theta_m + 273)^4\right] \tag{4}$$

with

$$\in_{eq} = \phi \cdot \varepsilon_m \cdot \varepsilon_f \tag{5}$$

For the bottom surface of a slab exposed to fire, the radiative shadowing can be ignored and the equivalent emissivity $\in_{eq}$ can be taken as equal to the emissivity of the floor material ε_m

(i.e. assuming $\phi = 1.0$ and $\varepsilon_f = 1.0$). However, the shadow effects for a downstand steel section may not be neglected given that the surfaces between the two flanges will not be exposed to the same incident radiation as the soffit areas of the bottom flange. To allow for reduced incident radiation to these surfaces and considering that the emissivity of steel is temperature-dependent rather than a constant codified value, the equivalent emissivity $\in_{eq}$ can be varied in the numerical simulations until the results are consistent with the experimental fire test data [17, 18]. Figure 3 illustrates the shadow effects on an open I-section along with the typical boundary conditions that have been applied in this study for a hybrid system.

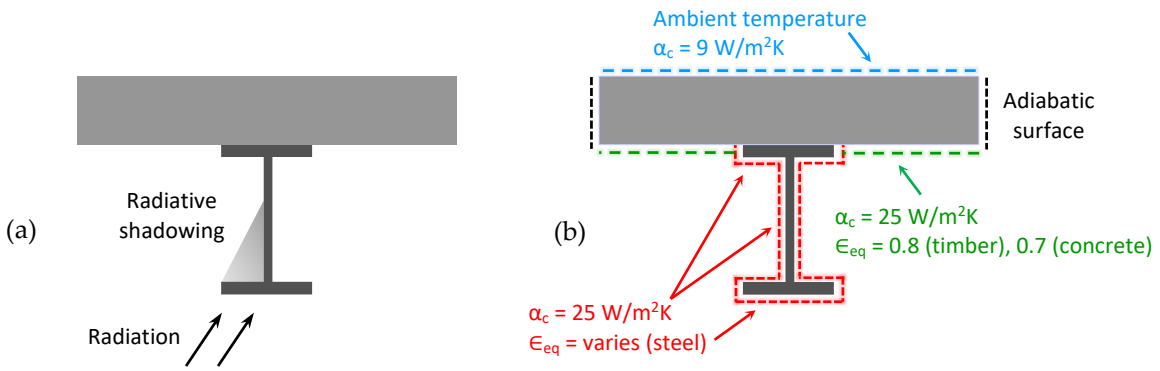

Figure 3: (a) Shadow effects on downstand steel beam, and (b) typical thermal boundary conditions of a hybrid beam for heat transfer simulation

There is currently a lack of experimental data on the thermal response of steel-timber hybrid beams in a downstand configuration. Fire test data for a slimfloor arrangement is available [19] but this is not particularly relevant to this study. Therefore, thermal models were initially developed and validated for standard furnace tests on a CLT floor [20] and a steel-concrete beam [21] to predict the temperature distribution measured by thermocouples located at different depths in the test specimens. Subsequently, the concrete flooring was substituted by timber to investigate the temperature distribution in a steel-timber beam and the results were juxtaposed with other existing thermal models documented in literature [2, 22]. In all cases, the thermal behaviour of the heated specimens was captured by using two-dimensional elements, but assuming one-dimensional heat transfer. This study is focused on the thermo-mechanical behaviour of steel-timber systems in a downstand arrangement. In the absence of targeted fire testing, it is reasonable to draw upon existing data from an analogous steel-concrete downstand system and to apply engineering judgment - particularly when developing or calibrating thermal models where the primary interest is in the heating response of the steel beam, rather than the timber slab. The limitations of this approach are clearly acknowledged, especially given that the CLT component is expected to influence the thermal response in ways distinct from concrete due to its combustibility. To address this, the study has considered a range of heating regimes (cooler top flange, uniform temperature profile, and hotter top flange) to reflect possible variations in heat exposure arising from the timber's contribution to the fire dynamics. This approach provides a conservative and

pragmatic basis for assessing steel performance in the early phases of model development, pending more targeted fire testing.

In regards to the fire exposure, a standard fire curve (ISO 834) has been selected on the basis that this is the most widely accepted benchmark available [23]. Standard fire curves have been known to be unscientific since their inception [24-26], and this is especially the case when the sample is combustible, as is the case for timber. This has been proven experimentally [27, 28]. Nonetheless, while other more scientifically sound methods exist – e.g. the compartment fire framework [29], Swedish curves [30], travelling fires [31], or large compartment fire framework [32] – none of these are suitable for combustible materials either and there is no widely accepted fire exposure for timber structures. As such, a standard fire curve was chosen instead since this is the more typical benchmark and there is some testing data available for timber systems. Ultimately, while the fire type will have some influence on the results, this study is primarily focused on the associated mechanical response and it is expected that a standard fire exposure will give a reasonable approximation for the thermal boundary conditions.

The thermal properties of materials are also needed to model heat transfer by conduction in structural fire engineering. These temperature-dependent parameters are density, specific heat and thermal conductivity. The values adopted in the simulations were based on the recommendations outlined in BS EN 1993-1-2 [33] for carbon steel, BS EN 1992-1-2 [34] for concrete and BS EN 1995-1-2 [9] for timber. In all cases, the four-noded linear heat transfer quadrilateral (DC2D4) element was used in the thermal simulations and a mesh size of around 5 mm was found to be satisfactory for the three materials, offering both computational efficiency and accuracy. This mesh discretization also closely aligns with the heat transfer simulations carried out by other researchers [35-37].

3.1.1 Thermal response of CLT floor

Fragiacomo et al. [20] experimentally investigated the out-of plane behaviour of CLT floors at both ambient and high temperatures. All test specimens were comprised of five layers with a width of 600 mm and a thickness of 150 mm, arranged in a lamella structure of 42-19-28-19-42 mm. One of the tests, involving a CLT specimen with its underside fully exposed to a standard fire, was simulated to capture the thermal response of timber in fire. Figure 4 illustrates the comparison of the temperature distribution between the heat transfer model and the measurements recorded by thermocouples at different depths within the specimen. The simulated temperature profiles are also consistent with the numerical results obtained by other researchers [20, 38, 39].

In general, it can be observed that the numerical results are in good agreement with the experimental data except for the temperature increase towards the end of the test. This is due to a change from one-dimensional to two-dimensional heat flux experienced by the highly deflected specimen on its sides as it approached failure. However, this response was not simulated because in a steel-timber hybrid beam with the CLT panels forming a continuous envelope, the heating can be assumed to be one-dimensional.

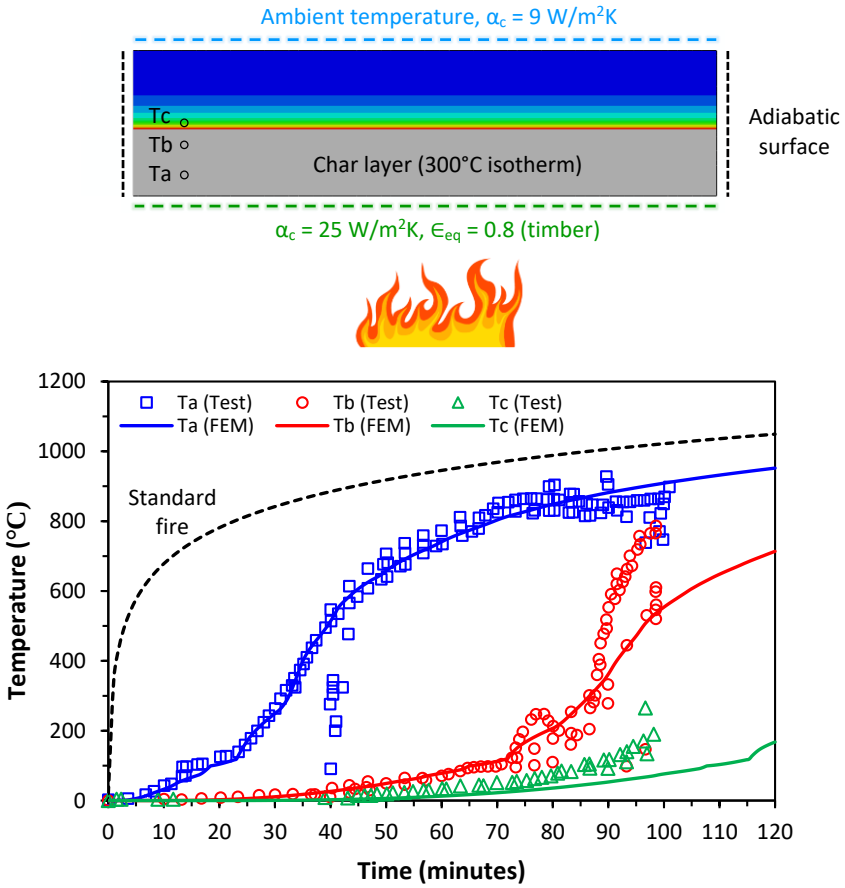

Figure 4: Comparison of temperature between experiment and numerical model (FEM) for CLT floor under standard fire conditions

3.1.2 Thermal response of steel-concrete beam

Zhang et al. [21] investigated the restrained behaviour of steel beams in steel-concrete composite systems exposed to increasing temperature in fire. In one of the specimens, the concrete slab, with a width of 1565 mm and a thickness of 120 mm, was connected to a downstand unprotected steel beam HN 250×125×6×9 using shear studs. The test was simulated to capture the thermal response of the specimen with its underside fully exposed to a standard fire. The equivalent emissivity of the steel beam was varied to consider radiative shadowing until the numerical results were consistent with the experimental fire test. The bottom flange and its sides were assigned a value of 0.7 whereas the remaining surfaces of the steel section were given a value of 0.4 to account for reduced radiation.

Figure 5 illustrates the comparison of the temperature distribution between the heat transfer model and the measurements recorded by thermocouples at different positions and depths in the experiment. For simplification, it is assumed that the temperatures of the bottom flange and the web are identical as any difference is negligible. In general, it can be observed that the numerical predictions are in good agreement with the experimental data. The simulated temperature profiles are also consistent with the numerical results obtained by Ding et al. [40].

Hence, the modelling approach is deemed to be satisfactory to capture the thermal response of a beam supporting a concrete slab in a downstand arrangement.

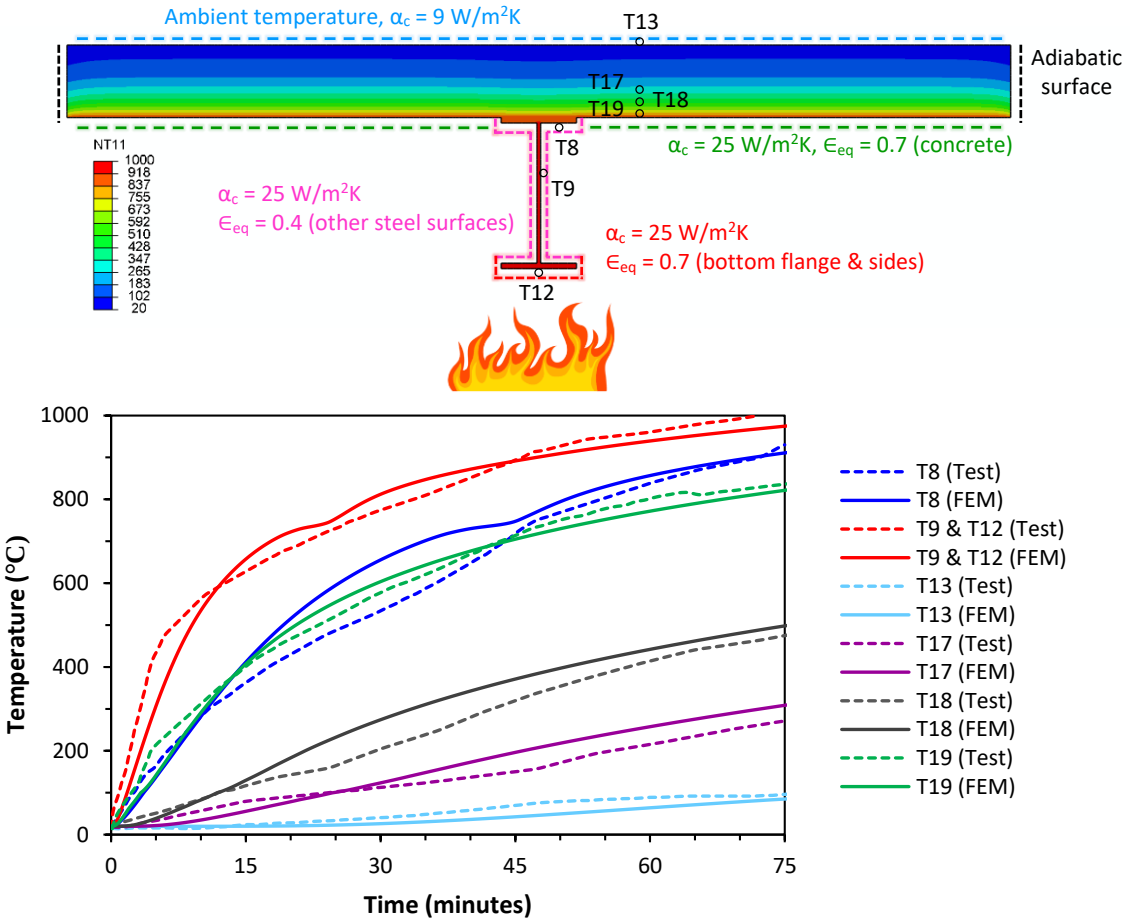

Figure 5: Comparison of temperature between experiment and numerical model (FEM) for steel-concrete beam under standard fire conditions

3.1.3 Thermal response of steel-timber beam

The thermal behaviour of a steel-timber beam is inherently more complex due to the combustibility of wood, and is by no means a simple heat transfer problem as seen previously for a steel beam supporting a non-combustible concrete slab. The burning behaviour of timber can be categorised into four important processes: pyrolysis, ignition, flaming combustion, and flame extinction [41]. When timber is directly exposed to a fire, it has the potential to alter the fire dynamics of a compartment by adding to the existing fuel load and increasing the temperature or total heat release rate of the enclosure, as evidenced by furnace tests conducted on steel beams with timber encapsulation [36] and large-scale mass timber fire tests [42, 43].

In consideration of the above discussion and the lack of experimental test data for a steel-timber downstand beam, the concrete slab mentioned in Section 3.1.2 was substituted with timber of density 480 kg/m^3 and 12 % moisture content to simulate the heat transfer. The thermal model assumes that the temperature within the furnace adheres to a standard fire

curve, including the energy released by burning of timber. In a furnace test, this is achieved by controlling the rate of fuel supplied to the burner to match the target standard fire curve; a similar approach was adopted in the test on the timber slab detailed in Section 3.1.1. This simplification also ensures that the standard fire thermal properties as defined in Eurocode 5 for timber can be used in the heat transfer analysis. In terms of the model boundary conditions, the equivalent emissivity of the steel is assumed to be 0.7 across the entire section as it is expected to receive radiation from the burning timber, thereby lessening the shadow effects. It is acknowledged that the standard fire conditions do not reflect a real fire in a combustible compartment with exposed timber and further research is required to investigate other fire scenarios as well. The likelihood of fire-induced delamination of CLT, which arises from the weakening of the bond line at elevated temperatures, is another phenomenon that can impact both the overall fire severity in a compartment and charring of timber, but not all CLT panels are susceptible to delamination, especially when face bonded using the new generation of adhesives that can maintain glueline integrity under heating [44-47]. Additionally, the North American standard ANSI/APA PRG 320 requires adhesive certification for CLT panels to ensure that delamination does not cause a secondary flashover. Hence, delamination is not considered within the scope of this study, similar to the approach adopted in investigation [22]. However, if delamination is observed during testing, it must be considered in future investigations as more research and fire test data on steel-timber hybrid systems become available. Hence, this study focuses on the use of relatively simple numerical models to simulate the heat absorption in a timber slab without an explicit consideration of factors such as wood combustion and delamination on the influence of the fire dynamics of an enclosure.

Figure 6 illustrates the comparison of the simulated temperature distribution between the steel-timber beam and the steel-concrete beam as outlined in Section 3.1.2. For simplification, it is assumed that the temperatures of the bottom flange and the web of the downstand steel beam are identical, as any difference is negligible. The temperature profiles in both slabs exhibit trends that are comparable to the in-depth temperature measurements recorded during the Epernon Fire Test Programme on combustible and non-combustible slabs [48]. Furthermore, the temperatures of the unprotected steel beam are also in good agreement with the thermal simulations performed by other researchers for steel-timber hybrid structures in a downstand configuration [2, 22]. Likewise, the results indicate that the top flange of the steel beam is cooler in a steel-concrete beam, indicating that concrete performs as more of a heat sink than timber under the assumed conditions in the heat transfer analysis. Consequently, concrete appears to offer better thermal protection to the steel beam during the fire exposure, reducing the rate of temperature rise in the steel section.

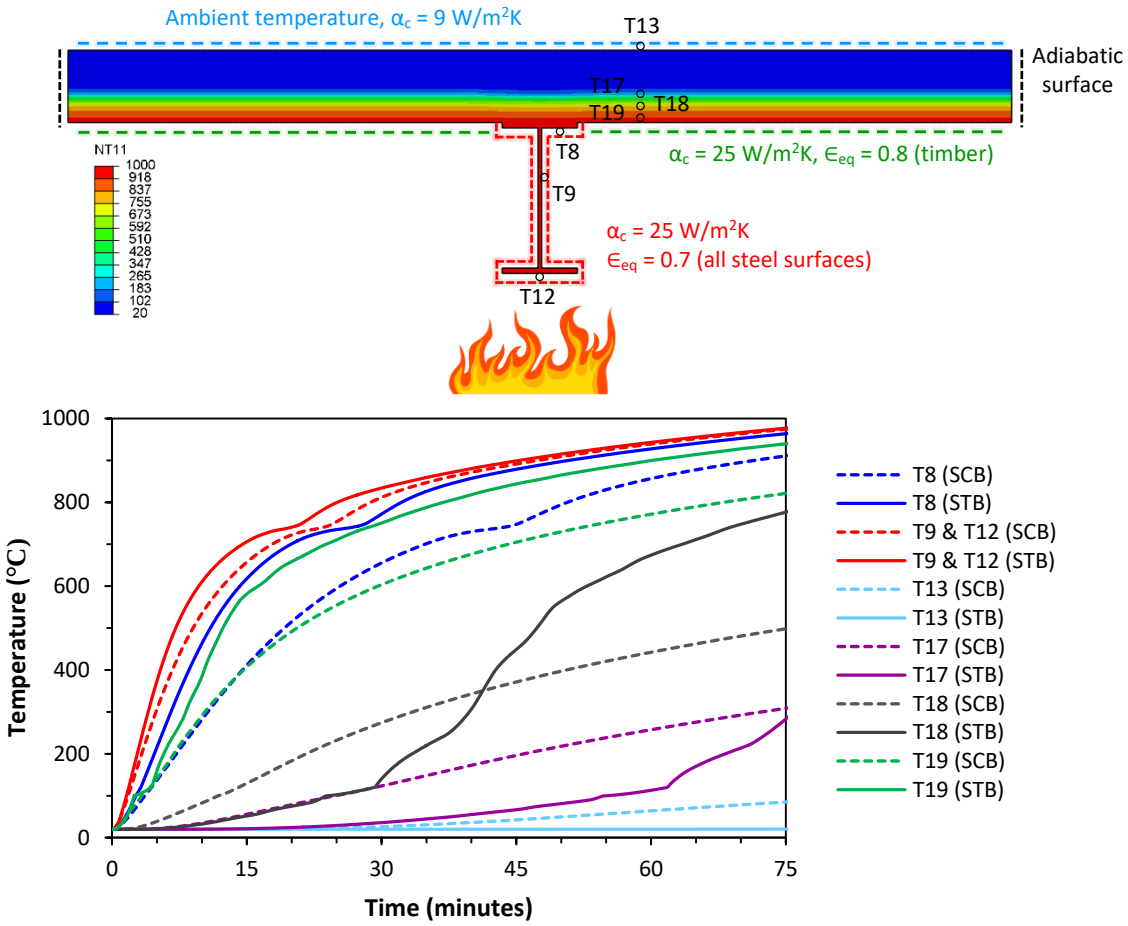

Figure 6: Comparison of simulated temperatures between steel-concrete beam (SCB) and steel-timber beam (STB) under standard fire conditions

3.2 Development and validation of high temperature mechanical model

If the temperature history from a heat transfer analysis or experiments is available, it is possible to simulate the mechanical response of a steel beam under fire conditions. This section presents the development of finite element models in *Abaqus* which are able to replicate the lateral-torsional buckling and axially restrained behaviour of heated steel beams. These models are then validated against experimental results found in the literature.

In the numerical simulations, the four-noded quadrilateral (S4R) shell element with reduced integration was adopted for meshing. The high-temperature material properties of carbon steel in terms of non-linear engineering stress-strain relationship and thermal expansion were in accordance with BS EN 1993-1-2 [33]. Two distinct types of end boundary conditions, as schematically depicted in Figure 7, were utilised. In Type 1, rigid body constraints connect all nodes of the web to a reference point, whilst the flanges have independent boundary conditions. This method can be used to model a simply supported member with ideal fork support conditions (prevent lateral and vertical translations including torsional rotation but allow warping of the flanges) at the ends. In Type 2, all nodes of the cross-section are

constrained to a reference point. This method can be used to model a member with axially and/or rotationally restrained conditions. The restraints to the steel beam were simulated using connector elements, which can define a connection between a node and a rigid body. The validation of the numerical models was performed through a comparison of the predictions with two sets of experimental data under fire conditions, one pertaining to the lateral-torsional buckling of an axially and laterally unrestrained beam [49], and the other to an axially and laterally restrained beam [3].

The high-temperature mechanical analysis consisted of two steps: an ambient-temperature loading step during which the load and a geometric imperfection were applied, followed by a heating step in which the temperature of the steel was increased according to a predefined temperature profile while maintaining the applied load. The geometric imperfection was included in the analysis by scaling an eigenmode of a linear buckling analysis on a perfectly straight beam. The static general solver including geometric nonlinearity was used in both steps. To ensure convergence during the thermal loading step, automatic stabilisation using dissipated energy fraction/damping factor and adaptive stabilisation were utilised in *Abaqus* to stabilise the unstable quasi-static problem, i.e. lateral-torsional buckling. Adaptive stabilisation was activated to control the ratio of viscous damping energy to the internal energy (ALLSD/ALLIE ≤ 5%) and to avoid inaccurate results. 5% is the default value in *Abaqus* for many situations because it is generally small enough not to significantly affect results, and was therefore retained to avoid introducing too many variables in the simulations.

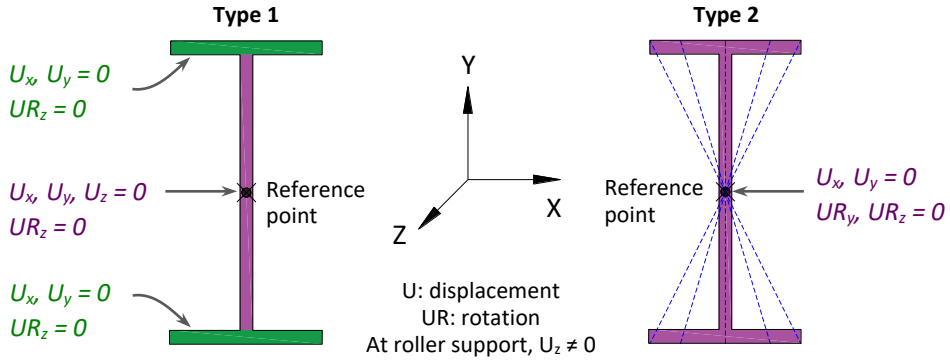

Figure 7: Beam end boundary conditions Type 1 and 2

3.2.1 Mechanical response of unrestrained steel beam

Mesquita et al. [49] investigated the lateral-torsional buckling behaviour of several fork supported IPE 100 beams at high temperatures. The span of the beams varied from 1.5 m to 4.5 m and three tests were carried out for each beam length. The beams were initially loaded and then uniformly heated at a constant rate of 800°C/h until failure by lateral-torsional buckling. The beams were made with steel having an average yield strength of 293.2 MPa. Figure 8 compares the numerical results obtained in this study, using Type 1 boundary conditions and a half-sine wave geometric imperfection, with the experimental data for the beam of 3.5 m span, as well as the predictions made by Kucukler [50]. Given the small size of

the specimen, a mesh size of 5 mm was adopted in the numerical model and an imperfection with a maximum amplitude of span/4000 was defined based on the measurements obtained from the tests. It can be observed that the numerical results are in good agreement with the measured path of the midspan deflection; the differences are imperceptible until 621°C. The results also align well with the predictions made by other researchers [51, 52]. This indicates that the simulation strategy adopted is able to mimic the lateral-torsional buckling response of steel beams in fire.

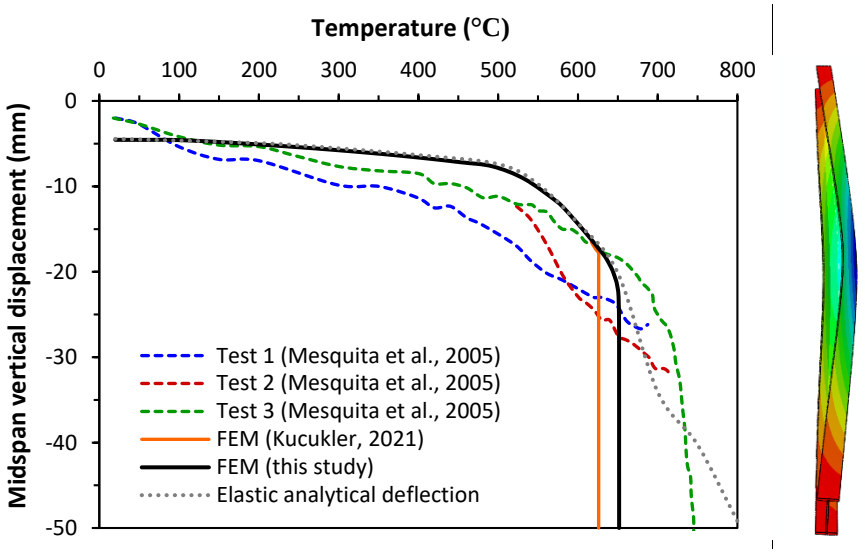

Figure 8: Comparison of displacement-temperature curves between experiment and numerical models (FEM)

3.2.2 Mechanical response of axially restrained steel beam

Li and Guo [3] investigated the fire performance of two restrained steel beams of H 250×250 ×8×12 section under non-uniform heating conditions. The beams were 4.5m and loaded with two point loads of 130 kN each. The average yield strength of the steel was 271 MPa. In one of the specimens, the axial (K_a) and end-rotational (K_r) stiffness of the beam were 39.5 kN/mm and 1.09 × 10^8 Nm/rad, respectively [53, 54]. This test was simulated using Type 2 boundary conditions and a mesh size of 20 mm was found to be satisfactory. A larger mesh was used in this case, in contrast to the 5 mm mesh used in the simulation outlined in Section 3.2.1, due to the greater steel cross-section and longer span of the specimen. Figure 9 shows the comparison between the numerical results obtained in this study and the experimental data in terms of the axial force and midspan vertical deflection. The predictions made by Zhang et al. [53] and Dwaikat and Kodur [55] are also illustrated. Overall, it can be inferred that the simulation strategy adopted is able to mimic the restrained behaviour of steel beams in fire using both axial and rotational restraint. The discrepancies between the test results and current predictions are mainly due to the simplified boundary conditions assumed in modelling the supports of the test.

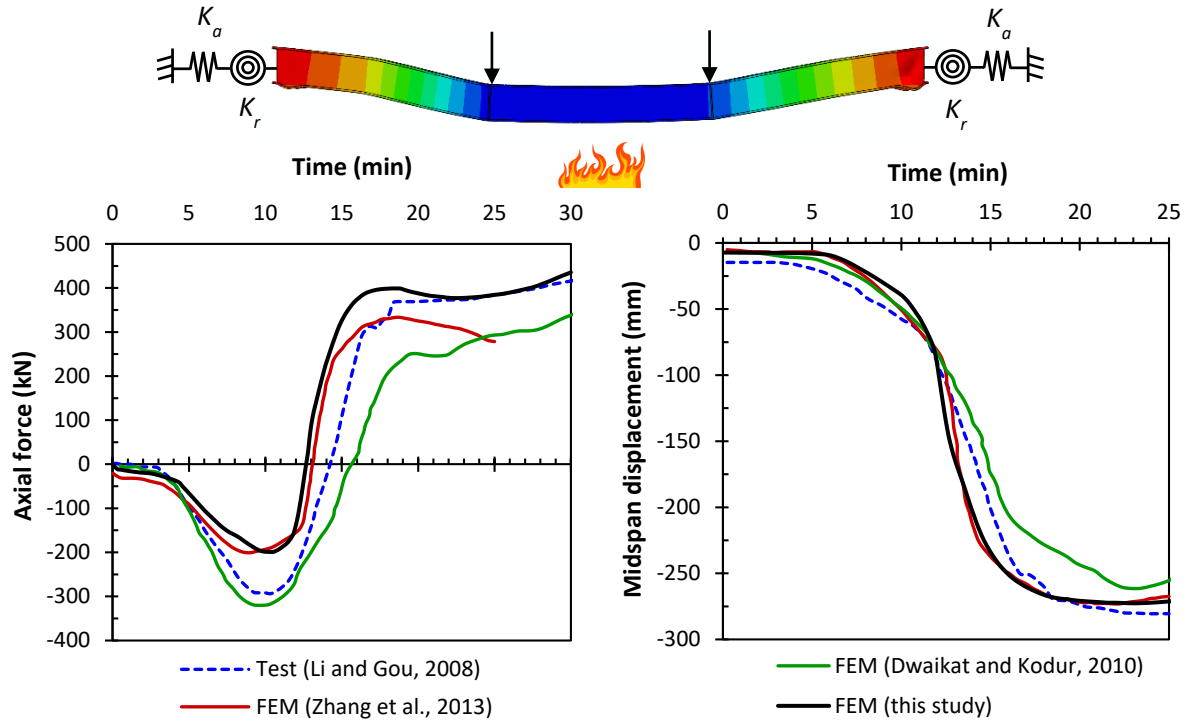

Figure 9: Comparison of axial force and displacement between experiment and numerical models

4. Parametric study

The validated numerical models were used to investigate the influence of some key parameters on the thermo-mechanical response of unprotected steel beams in steel-timber hybrid structures. As explained earlier in Section 1, the CLT slab is not incorporated in the mechanical models. However, this modelling assumption adheres to a conservative approach that is in line with current design practice and helps to develop new insights on the structural response of steel-timber hybrid structures in fire. The parameters considered are: (i) the degree of lateral restraint provided by the fasteners, (ii) the axial restraint of the end connections, and (iii) the beam temperature distribution under both uniform and non-uniform heating scenarios. Following the description given in Section 3.2, the high-temperature mechanical analysis consisted of two steps: an ambient-temperature loading step followed by a heating step in which the temperature of the steel was increased accordingly while maintaining the applied load.

A hot-rolled steel beam of section UB 457×152×74, grade S355 and 9m span was chosen for the investigation. The 9 m span, giving a span-to-depth ratio of 19.5, was selected to reflect a central secondary beam in a typical steel framing scheme with 9 m × 9 m column grids for a conventional commercial office floor. In terms of applied loading, the dead load is assumed to be 3.0 kN/m² (including self-weight of slab, finishes, and services) and the live load is taken as 5.0 kN/m². Hence, the top flange of the beam is assumed to be loaded with a line load of 24.75 kN/m at the fire limit state from a tributary width of 4.5 m of the slab, giving a load ratio of 0.44 if the beam is assumed to be fully laterally restrained at ambient temperature. The load

ratio is defined as the ratio of the applied moment at the fire limit state to the plastic moment capacity of the member at ambient temperature (load level in BS EN 1994-1-2 [56]). This study considers only one load ratio, but future work should explore a wider range to more accurately reflect the broader load conditions present in real steel-timber hybrid structures.

4.1 Lateral and axial restraint

From the experimental investigations described in Section 2 to quantify the longitudinal shear behaviour of steel-to-timber connections, the range of lateral stiffness K_{ser} was found to vary approximately between 1500 N/mm to 3500 N/mm for the tested screws. At the fire limit state, K_{fi} can be assumed to vary between 200 N/mm to 467 N/mm in accordance with Eurocode 5 guidance. Hence, a range of lateral restraint K_{fi} was selected for the parametric study: 10 N/mm, 25 N/mm, 100 N/mm, 200 N/mm, 500 N/mm, and ∞ (full lateral restraint). Low values of K_{fi} were also included to investigate the sensitivity of the beam to the effect of low lateral restraint.

Experimental investigations on screws of equal diameter in steel-to-timber connections have demonstrated a range of failure modes, from brittle to typically ductile responses [6]. Therefore, modelling the screw connections as linear elastic-perfectly brittle was adopted as a conservative worst-case design scenario. Additionally, Eurocode 5 specifies a single slip modulus value K_{fi} for screws in fire, which is intended to be both practical and conservative. As such, a sensitivity analysis using alternative models (e.g. bilinear or including temperature-dependent degradation) was not conducted, since reliable experimental data across a sufficient temperature range for this connection type is unavailable, and the intent is to establish a conservative baseline rather than to explore a broader range of screw behaviours. In all cases, it is assumed that the screws are: (i) linear elastic but fail in a brittle manner with a shear deformation capacity of 15 mm, and (ii) staggered at equal spacing of 250 mm on the top flange of the beam. BS EN 26891 [11] recommends that push-out tests may be stopped when the ultimate load is reached, or when the slip is 15 mm, whichever occurs first. Hence, an ultimate slip of 15 mm was adopted for the parametric study in the absence of connection test data in fire and also due to the fact that some of the screws tested in [6] experienced slippage of at least 15 mm along with brittle failure at ambient temperature.

The influence of varying degrees of axial restraint provided by the end connections was also investigated. Seven levels of axial restraint were considered: $0.05K_a$, $0.15K_a$, $0.30K_a$, $0.50K_a$, $1.00K_a$, and ∞ (full axial restraint), where K_a is the axial stiffness of the beam at ambient temperature and is found to be 221 kN/mm. The axial restraint is assumed to be linear and unaffected by temperature. The effect of lateral and axial restraint is simulated using connector elements, following the similar approach adopted in Section 3.2. Figure 10 illustrates the location of lateral and axial restraint for the beam as part of the parametric study.

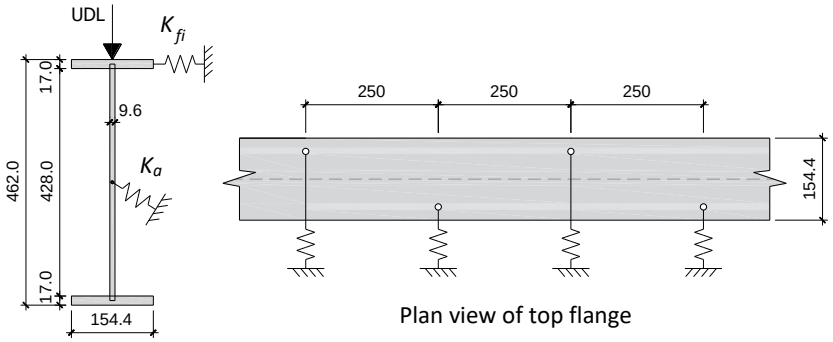

Figure 10: Position of lateral (K_{fi}) and axial (K_a) restraint for parametric study

4.2 Temperature distribution

In line with the simulation procedure explained in Section 3.1, the thermal response was obtained for the beam supporting a typical 160 mm CLT slab with a density of 480 kg/m^3 and a moisture content of 12%. The width of the slab is assumed to be 1000 mm in the numerical model for computational efficiency (modelling the whole span length does not affect the heat transfer analysis) and thermal boundary conditions are as explained previously. The underside of the CLT is assumed to be fully exposed to a standard fire without any encapsulation. In a real building fire with a decay phase, the actual heating rates will be different, but the adopted temperature regimes in this study will help to obtain an understanding of the structural response of the beam leading to failure, although to a different timescale.

Figure 11 illustrates the simulated non-uniform temperature distribution of the steel-timber beam in which the web and bottom flange are assumed to have the same temperature while the top flange is cooler due to the heat sink effect of the timber slab. Given the lack of experimental data for such hybrid systems in fire, it is also assumed that the temperature distribution in the beam is uniform, in which the whole section is taken to be at the temperature of the web. This is a more conservative assumption with a hotter compression flange for the design of steel-timber hybrid structures. It is important to reiterate that this study focuses on relatively simple heat transfer analysis and there is a clear need for complementary experimental work to understand the thermal response of steel-timber beams in fire with coupled interaction between the structural elements and resulting fire dynamics.

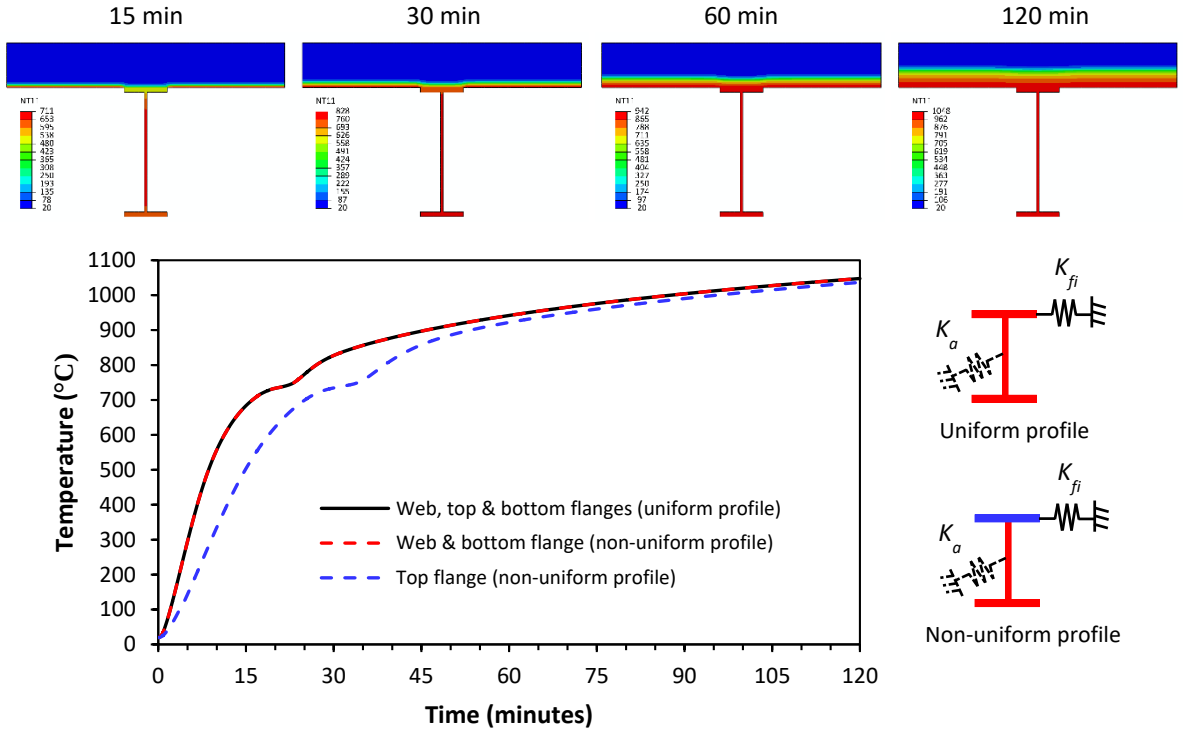

Figure 11: Temperature profiles adopted for parametric study

4.3 Mesh sensitivity analysis

To further complement the validation studies presented in Section 3.2, a comparison was made between the critical elastic buckling moment of the beam with lateral restraint for various eigenmodes in *Abaqus* and *LTBeamN* [57], which is commonly used for linear buckling analysis. This was done to verify the numerical results from the two softwares in the absence of high temperature test data of steel-timber downstand beams. A mesh sensitivity analysis was conducted in two steps to ascertain the optimal mesh size for the parametric study: (i) linear buckling analysis, and (ii) non-linear thermo-mechanical analysis. A finer mesh typically results in a more accurate solution but the simulation becomes more computationally expensive.

4.3.1 Linear buckling analysis

In the linear buckling analysis, mesh sizes ranging from 40 mm to 5 mm were used to verify the elastic buckling moments of the steel beam with elastic lateral restraint of 200 N/mm (without brittle failure) at 250 mm spacing. The results obtained are summarised in Table 1. It can be observed that the results from *Abaqus* are slightly lower than those given by *LTBeamN*. This is largely due to the fact that the fillet radius of the steel beam was not explicitly modelled in *Abaqus* to reduce the complexity of the model, and that reduced integration was also considered in the shell elements. Nevertheless, a mesh size of 20 mm gives an error of less than 2.5% for the first eigenmode. Figure 12 illustrates the first three buckling modes of the beam under both unrestrained conditions and partially restrained conditions with closely-

spaced top flange lateral restraint. The first eigenmodes were also used to perform an imperfection sensitivity analysis, as elaborated later in Section 4.4.

Table 1: Critical buckling moment in *Abaqus* and *LTBeamN* with K_{fi} = 200 N/mm

Eigenmode	Critical buckling moment (kNm)					
	LTBeamN	Abaqus with different mesh sizes (mm)				
		40	30	20	10	5
1	1035	1004	1005	1012	1014	1017
2	1116	1087	1088	1089	1090	1092
3	1822	1688	1689	1694	1693	1695

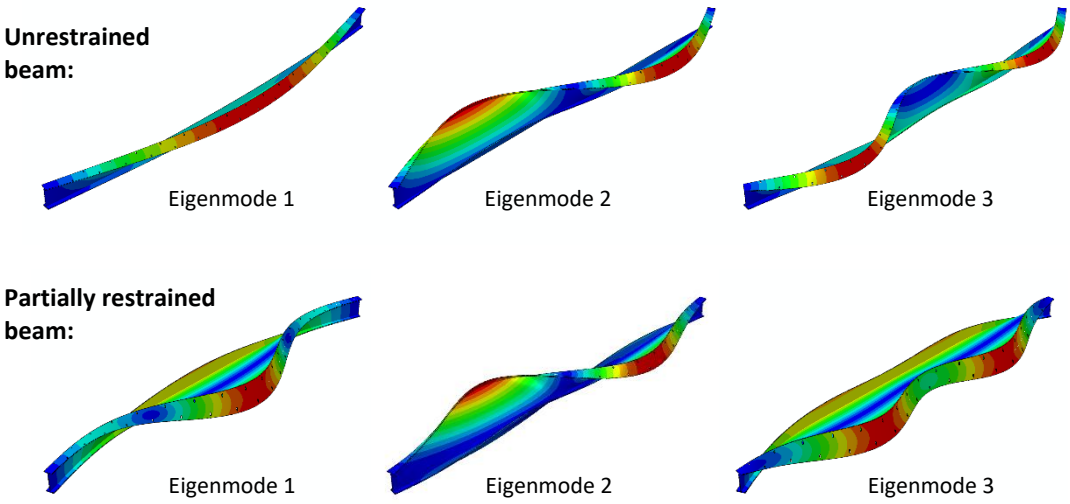

Figure 12: Typical buckling modes for unrestrained and partially restrained beams

4.3.2 Non-linear thermo-mechanical analysis

In the non-linear thermo-mechanical analysis, mesh sizes ranging from 40 mm to 10 mm were selected for a further mesh sensitivity analysis (the 5 mm mesh was omitted as it proved to be too computationally expensive). The steel beam was loaded with a line load of 24.75 kN/m and subjected to a uniform increase in temperature as described in Section 4.2. The geometric imperfection was initially considered using the conventional half-sine wave of an unrestrained beam. A constant elastic lateral stiffness of 200 N/mm without the 15 mm fracture limit was adopted to avoid convergence issues at this stage of the analysis. The failure temperature is taken as the temperature at which the vertical deflection reaches span/20 irrespective of the magnitude of the lateral deflection. The results of this analysis are summarised in Table 2. Considering the minimal variability between the failure temperatures,

a mesh size of 20 mm was ultimately selected for the parametric study, which also adequately simulated the test beam in Section 3.2.2.

Table 2: Failure temperature for different mesh sizes with K_{fi} = 200 N/mm

Mesh size (mm)	**40**	**30**	**20**	**10**
Number of elements	9,622	11,514	19,321	69,644
Failure temperature (°C)	573.7	574.6	574.3	574.2

4.4 Imperfection sensitivity analysis

Material and geometric imperfections can influence the stability of structural members. Residual stresses, which are generated from the manufacturing process, have been neglected in this investigation as this form of material imperfection decreases with higher temperature levels in a fire. In addition, Vila Real et al. [58] and Kucukler [50] have demonstrated that the buckling resistance of beams is less sensitive to residual stresses with increasing temperature. Residual stresses have also been omitted in other high temperature numerical simulations including restrained conditions [59-61]. While this assumption holds at lower load levels due to the negligible influence of residual stresses, their inclusion is recommended at load ratios around 0.65 of the load-bearing capacity at ambient temperature, where their effects become significant in numerical analyses [62]. In the parametric study, the applied load ratio is 0.44, which is sufficiently low to justify the exclusion of residual stresses from the analysis.

Geometric imperfection, due to manufacturing, transportation or handling processes, were incorporated in the analysis by performing a prior linear buckling analysis and scaling the buckling eigenmode as necessary. A lateral geometric imperfection based on the first lateral-torsional buckling mode of the beam was considered with a maximum amplitude of 1/1000 of the beam length. This value was adopted based on previous numerical studies [49, 50, 59-61, 63]. It was found that the failure temperature was sensitive to the type of imperfection applied, thus a sensitivity analysis was performed to seek the suitable imperfection type. Similarly, Couto and Vila Real [63] also demonstrated that the shape of the imperfection affects the lateral-torsional buckling resistance of a steel beam. The following imperfections were considered:

- **Imperfection 1**: first eigenmode of a laterally unrestrained beam (half-sine wave);
- **Imperfection 2**: first eigenmode of a partially laterally restrained beam based on K_{fi}.

Table 3 illustrates the effect of the imperfection type on the failure temperatures of the beam for the practical range of K_{fi} from 200 N/mm to 500 N/mm. It is typical to assume full lateral restraint at ambient-temperature for the beam due to the high lateral stiffness values of K_{ser} and test observations [5]. However, small lateral movements might occur in the simulations which could affect the shape and magnitude of the imperfection. Hence, the use of the full lateral restraint conditions at the ambient-temperature loading step was also considered. This differs from the simulation outlined in Section 4.3.2, where K_{fi} rather than the full lateral restraint was applied at ambient temperature, which resulted in a subsequent distortion of

the imperfection for the mechanical analysis in fire. Imperfection 2 was eventually selected for the parametric study as it results in the lowest failure temperatures.

Table 3: Effect of imperfection type on predicted failure temperature

K_{fi} (N/mm)	Failure temperature (°C)	
	Imperfection 1	Imperfection 2
200	580	568
500	593	574

5. Results and discussion

This section presents the numerical results of the parametric study under the influence of various parameters. Also, the simulations now take into consideration the 15 mm fracture limit of the lateral restraint. This was intentionally omitted in the previous models described in Section 4 to avoid convergence issues during the analysis.

5.1 Influence of lateral restraint on axially unrestrained steel beams (K_a = 0)

Secondary steel beams are generally designed as simply supported members at ambient temperature. This section explores the influence of lateral restraint on the lateral-torsional buckling behaviour of simply supported beams in fire. In the numerical simulations, a Type 1 boundary condition was adopted to ensure that the beam is axially unrestrained and can expand freely during the heating phase.

Figure 13 compares the midspan vertical deflections of the chosen beam for various levels of lateral stiffness K_{fi} of the screw connections and considering both the uniform and non-uniform temperature profiles. The deflection-temperature results are also compared to the fully laterally restrained case, as well as to the hand calculated elastic deflection of the beam under uniform heating. The failure line corresponding to the midspan vertical deflection of span/20 is also presented.

It can be observed that the beam is sensitive to low levels of lateral restraint. For both the uniform and non-uniform heating cases, the low lateral restraint (10 N/mm) leads to a much lower runaway deflection temperature than all the other cases. All the other partial lateral restraint levels (equal to or above 100 N/mm) result in similar runaway deflection temperatures. In uniformly heated cases, lateral-torsional buckling leads to runaway deflection at an earlier stage than it does in non-uniformly heated cases, in which the response is closer to the fully laterally restrained beam as the cooler compression flange provides enhanced structural performance in fire but this behaviour is expected to vary across various assumed temperature scenarios. The effect of thermal bowing can also be observed due to the uneven temperature distribution. However, the simply supported behaviour does not accurately reflect the actual thermo-mechanical response under fire conditions as it fails to account for the axial restraint provided by adjacent structures.

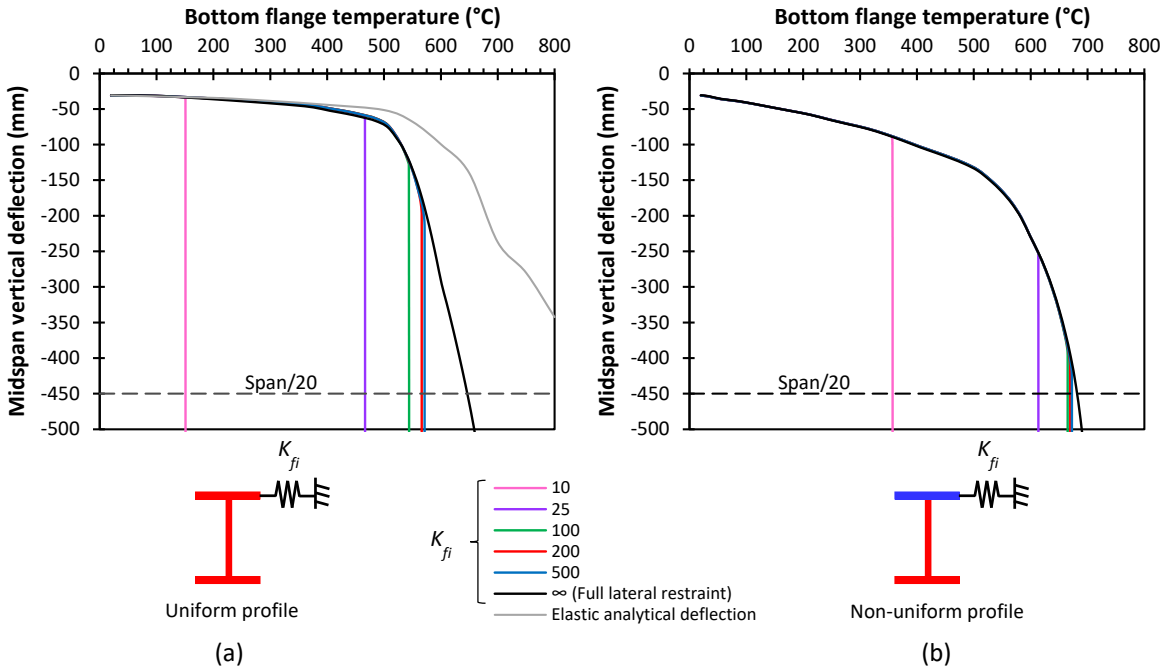

Figure 13: Vertical deflection-temperature relationships under varying lateral stiffness K_{fi} for (a) uniform temperature profile and (b) non-uniform temperature profile

5.2 Influence of lateral restraint on axially restrained steel beams ($K_a \neq 0$)

In real structures, it is well-established that the surrounding connections generally restrict thermal expansion and induce axial compression force followed by tensile force in a fully laterally restrained steel beam exposed to fire [4, 60]. The introduction of catenary forces in a fully laterally restrained beam provide an additional mechanism to resist the external loading at high temperature as material degradation occurs and bending resistance decreases.

In this section, the influence of varying degrees of axial restraint provided by the end connections under both uniform and non-uniform heating is investigated for a K_{fi} value of 200 N/mm. Seven levels of axial restraint are considered: $0.05K_a$, $0.15K_a$, $0.30K_a$, $0.50K_a$, $1.00K_a$, and ∞, where K_a is the axial stiffness of the beam at ambient temperature and is found to be 221 kN/mm. The axial restraint is assumed to be linear and unaffected by temperature. Figure 14 (a) to (f) illustrate the evolution of the midspan vertical deflection of the bottom flange and midspan lateral deflection of the top flange along with the axial force development for various axial restraint and temperature distributions. The vertical deflection-temperature and axial force-temperature relationships are also compared to a fully laterally restrained beam ($K_{fi} = \infty$) for the corresponding axial restraint. In some cases, the full thermo-mechanical response could not be captured due to convergence difficulties encountered in the large-displacement analysis.

In general, it can be observed that in the presence of axial restraint, a partially laterally restrained beam initially follows a similar gradient to the fully laterally restrained beam but subsequently undergoes the classical runaway deflection due to lateral-torsional buckling. This is clearly visible in Figure 14 (c) and (d) where there is a sudden increase in lateral

deflection in the midspan region. A turning point is then reached when the rate of runaway deflection is attenuated due to the development of tensile force in the member, where it starts to behave as a cable. Additionally, the axial-temperature relationships illustrated in Figure 14 (e) and (f) indicate that the curves follow similar gradients to the fully laterally restrained beam until a maximum compression force is attained.

As expected the imposition of higher levels of axial restraint reduces the failure temperature at which the beam undergoes instability by lateral-torsional buckling. It is also evident that it is unsafe to assume fully laterally restrained conditions in fire. In general, the thermo-mechanical response of partially laterally restrained beams with end axial restraint can be described as follows:

- Initially, the beam follows the behaviour of a fully laterally restrained beam until a maximum compressive force is reached when the first screw fails in shear in the midspan region.
- Once the first screw fails, the remaining screws start to fail in succession and the beam undergoes runaway deflection whereby there is a rapid increase in both vertical and lateral deflections along with a very sharp transition from compressive to tensile force in the member.
- The catenary stage is then reached and the tensile force generated provides the mechanism to slow down the rate of runaway midspan deflection. The tensile force remains at a fairly constant magnitude up to a maximum until failure occurs when the tensile capacity of the beam is exceeded.

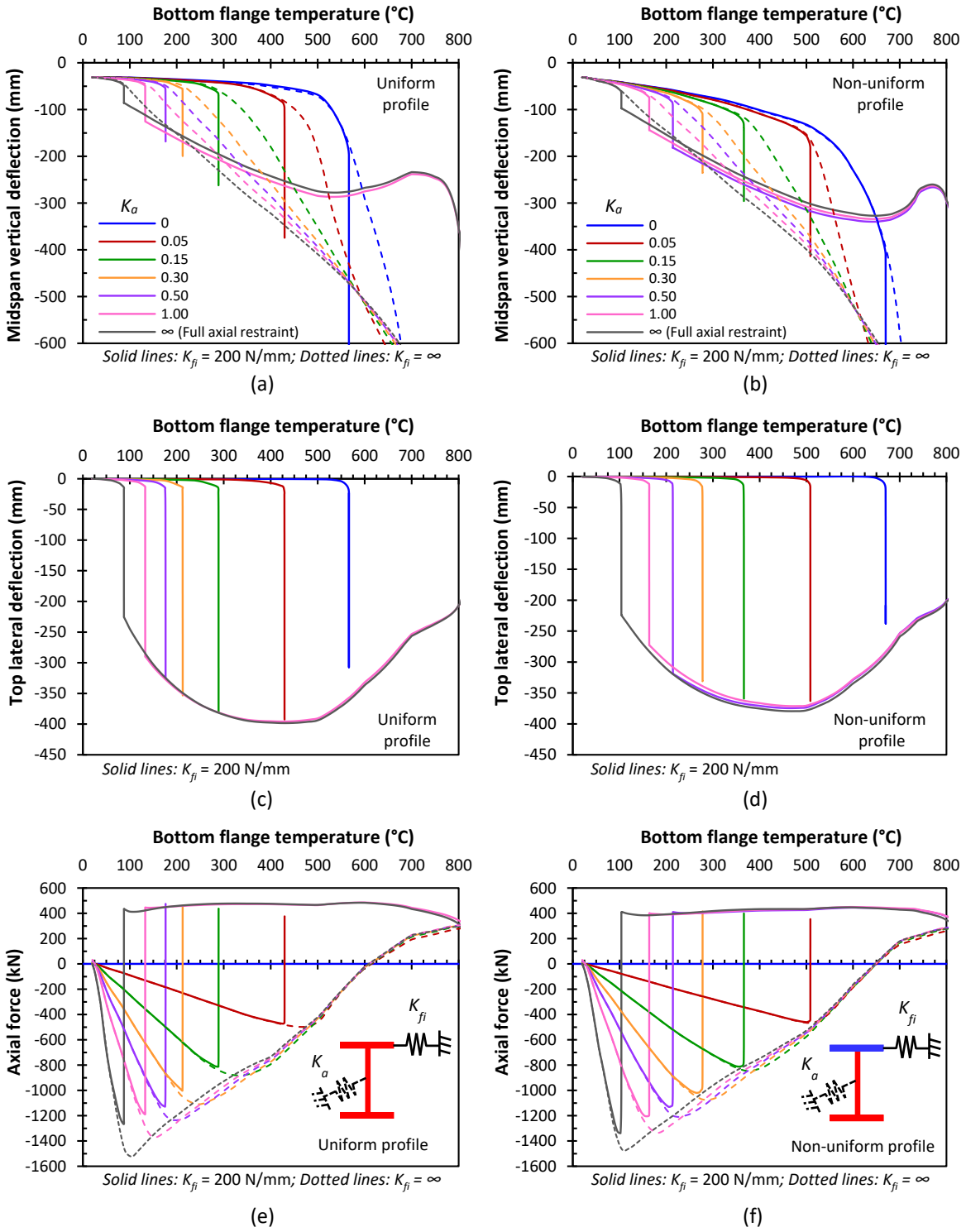

Figure 14: Temperature relationships for (a, b) midspan vertical deflection, (c, d) top flange lateral deflection, and (e, f) axial force with varying axial restraint under uniform and non-uniform temperature profiles for K_{fi} = 200 N/mm and K_{fi} = ∞

Figure 15 shows the variation of the induced axial forces in the beam under different degrees of lateral restraint coupled with uniform and non-uniform temperature distributions. In all cases, the axial restraint level is assumed to be equal to the axial stiffness of the beam at ambient temperature ($1.00K_a$). The trends in the results are remarkably consistent with the

axial force development in Figure 14 and it can be observed that the imposition of higher levels of lateral restraint increases the failure temperature at which the beam becomes unstable by lateral-torsional buckling. Also, there is no significant difference in the failure temperatures between the uniform and non-uniform heating regimes under the same axial restraint level.

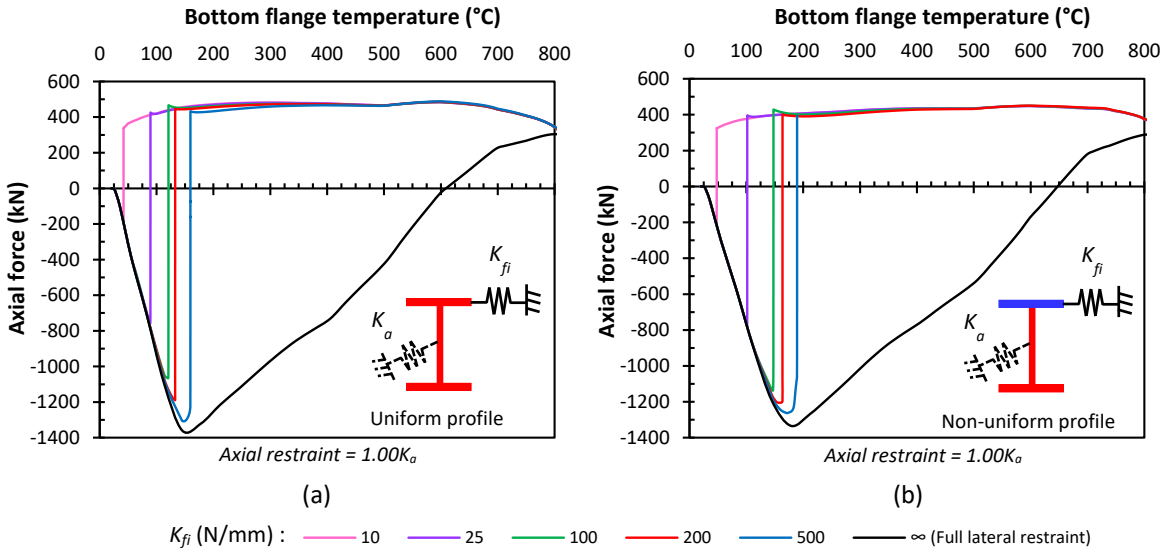

Figure 15: Axial force-temperature relationships under varying lateral stiffness K_{fi} and constant axial restraint of $1.00K_a$ for (a) uniform temperature profile and (b) non-uniform temperature profile

5.3 Comparison of failure temperatures

According to guidance documents [15, 64], construction elements must provide one or more of the performance criteria during a specified fire exposure, namely: (a) load resistance or stability, (b) thermal insulation, and (c) integrity. Allied to this, steel-timber hybrid structures must sustain mechanical loads without exceeding large deflections and disproportionate collapse, limit the temperature rise on the unexposed side of the CLT slab and prevent the passage of flames and hot gases through cracks or gaps in the timber floor structure. The CLT slabs must demonstrate compliance with (a), (b) and (c) whereas the steel beams are only required to satisfy the load bearing capacity criterion. For this study, the failure temperature of the steel beam is therefore taken as either of the following, whichever is exceeded first:

- vertical deflection of span/20 in accordance with BS 476-20 [65]; or
- the temperature at which runaway deflection starts leading to large lateral displacements.

Figure 16 illustrates the failure temperatures of the beam with various axial restraint under the heating regimes described in Section 4.2 as well as a new case in which the top flange is assumed to be hotter by 10% than the web and bottom flange. This is intended to represent a situation where the burning CLT slab can potentially result in a higher temperature of the compression flange. It can be observed that the failure temperature for this particular scenario

is marginally lower than the correspondingly uniformly heated case. As the axial restraint increases, the failure temperature decreases due to increase in axial compression caused by restrained thermal expansion. Hence, the use of steel frame connections that provides sufficient axial ductility to accommodate thermal expansion should be favoured in steel-timber hybrid structures.

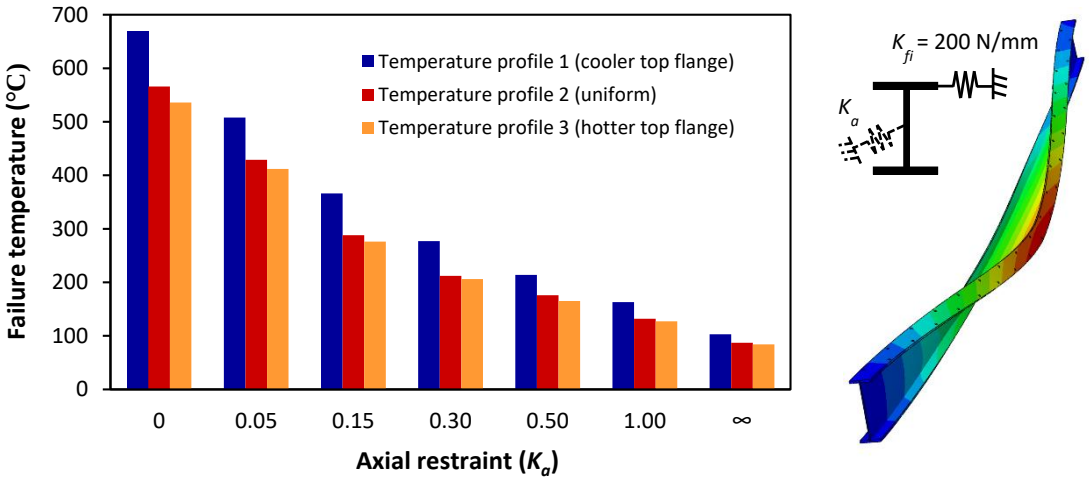

Figure 16: Failure temperature with varying axial restraint and temperature profiles under constant lateral restraint K_{fi} = 200 N/mm

6. Conclusions

This paper presents results illustrating the influence of lateral and axial restraint on the lateral-torsional buckling behaviour of secondary steel beams in steel-timber hybrid structures at high temperature, considering different heating regimes and mechanical behaviour of the steel-to-timber fixing screws. Based on the results of this investigation, the following conclusions can be drawn:

- In the simply supported condition (no axial restraint), all the partially laterally restrained beams with lateral restraint equal to or above 100 N/mm experience failure temperatures close to those of the fully laterally restrained cases. This level of lateral stiffness is easily achieved by any practical arrangement of 12 mm diameter fixing screws.
- A partially laterally restrained beam (i.e. restraint stiffness of 10 to 500 N/mm) with axial restraint initially behaves similarly to a corresponding fully laterally restrained beam until failure of the first screw occurs in the midspan region. The beam subsequently undergoes runaway deflection due to lateral-torsional buckling until there is an abrupt transition from compression to tension; the development of the catenary action attenuates the runaway deflection until failure occurs when the tensile capacity of the beam is reached.
- Restrained thermal expansion further decreases the failure temperature of a partially laterally restrained beam. It is recommended to adopt steel frame connections with

adequate axial ductility and low axial stiffness to accommodate the thermal expansion in steel-timber hybrid structures.

- The results indicate that designing beams in steel-timber hybrid structures as laterally unrestrained in fire is conservative. On the other hand, it is not realistic to assume fully laterally restrained conditions in fire pursuant to the Eurocode 5-based screw characteristics.
- Screws play a crucial role in the fire safety of steel-timber hybrid structures and further testing is required to fully characterise their behaviour in burning timber.
- Further research is required to expand the range of parameters considered. Such work should first be supported by experimental data, especially given the current limited understanding of the local behaviour of screws and the overall performance of steel-timber hybrid systems in fire. Studies to investigate the effect of realistic fire scenarios (heat sink effect and/or radiation of the CLT and its effects on the local temperature distribution in the steel profile), load ratios, and slenderness ratios are required both experimentally and numerically.

Acknowledgements

This work was supported by the UK Engineering and Physical Sciences Research Council [grant number EP/T517835/1] in collaboration with OFR Consultants. For the purpose of open access, the author has applied a Creative Commons Attribution (CC BY) licence to any Author Accepted Manuscript version arising from this submission.

Declaration of competing interest

The authors declare that they have no known competing financial interests or personal relationships that could have appeared to influence the work reported in this paper.

Author Contributions

Aatish Jeebodh: Conceptualization, Methodology, Software, Validation, Formal analysis, Data Curation, Writing - original draft, and Visualization. **Buick Davison, Martyn S. McLaggan, Ian Burgess, Danny Hopkin, and Shan-Shan Huang**: Conceptualization, Methodology, Writing - review & editing, Supervision, Project administration, and Funding acquisition.

References

[1] D. Barber *et al.*, "Design Guide 37: Hybrid Steel Frames with Wood Floors," American Institute of Steel Construction, USA, 2022.

[2] D. Barber, A. Roy-Poirier, and L. Wingo, "Modelling the fire performance of steel beam to CLT connections for hybrid construction," in *Proceedings of the 12th Asia-Oceania symposium on fire science and technology (AOSFST 2021)*, Brisbane, Australia, 2021, doi: https://doi.org/10.14264/E58A1CA.

[3] G.-Q. Li and S.-X. Guo, "Experiment on restrained steel beams subjected to heating and cooling," *Journal of Constructional Steel Research,* vol. 64, no. 3, pp. 268-274, 2008/03/01/ 2008, doi: https://doi.org/10.1016/j.jcsr.2007.07.007.

[4] Y. Wang, I. Burgess, F. Wald, and M. Gillie, *Performance-Based Fire Engineering of Structures*. Taylor & Francis, 2012.

[5] H. Merryday, M. Potuzak, D. Roueche, and K. Sener, "Experimental and Numerical Investigations on the Usage of CLT Panels to Form Timber-Steel Composite Floor Systems," in *World Conference on Timber Engineering (WCTE 2023)*, Oslo, Norway, 2023, pp. 3373-3381, doi: https://doi.org/10.52202/069179-0439.

[6] H. C. Merryday, K. Sener, and D. Roueche, "Pushout Tests on Steel-Timber Connections Using Self-Tapping Screws," *Structures Congress 2023,* pp. 312-327, 2023, doi: https://doi.org/10.1061/9780784484777.028.

[7] A. Hassanieh, H. R. Valipour, and M. A. Bradford, "Experimental and numerical investigation of short-term behaviour of CLT-steel composite beams," *Engineering Structures,* vol. 144, no. C, pp. 43-57, 2017, doi: https://doi.org/10.1016/j.engstruct.2017.04.052.

[8] BS EN 1995-1-1:2004+A2, *Eurocode 5: Design of Timber Structures - Part 1-1: General - Common Rules and Rules for Buildings*. British Standards Institution, 2014.

[9] BS EN 1995-1-2, *Eurocode 5: Design of Timber Structures - Part 1-2: General - Structural Fire Design*. British Standards Institution, 2004.

[10] A. Jeebodh, B. Davison, M. S. McLaggan, I. Burgess, D. Hopkin, and S.-S. Huang, "Influence of continuous elastic lateral restraints on beams and beam-columns of steel-timber hybrid structures in fire," *Fire Safety Journal,* vol. 146, p. 104172, 2024/06/01/ 2024, doi: https://doi.org/10.1016/j.firesaf.2024.104172.

[11] BS EN 26891, *Timber structures. Joints made with mechanical fasteners. General principles for the determination of strength and deformation characteristics*. British Standards Institution, 1991.

[12] A. Asiz and I. Smith, "Connection system of massive timber elements used in horizontal slabs of hybrid tall buildings," *Journal of Structural Engineering,* vol. 137, no. 11, pp. 1390-1393, 2011, doi: https://doi.org/10.1061/(ASCE)ST.1943-541X.0000363.

[13] Abaqus, "Abaqus/CAE User's Guide," Dassault Systèmes, 2021.

[14] J. F. Sacadura, "Radiative heat transfer in fire safety science," *Journal of Quantitative Spectroscopy and Radiative Transfer,* vol. 93, no. 1, pp. 5-24, 2005/06/15/ 2005, doi: https://doi.org/10.1016/j.jqsrt.2004.08.011.

[15] BS EN 1991-1-2, *Eurocode 1: Actions on structures - Part 1-2: General actions - Actions on structures exposed to fire*. British Standards Institution, 2002.

[16] J. I. Ghojel and M. B. Wong, "Heat transfer model for unprotected steel members in a standard compartment fire with participating medium," *Journal of Constructional Steel Research,* vol. 61, no. 6, pp. 825-833, 2005/06/01/ 2005, doi: https://doi.org/10.1016/j.jcsr.2004.11.003.

[17] J. M. Franssen, G. M. E. Cooke, and D. J. Latham, "Numerical simulation of a full scale fire test on a loaded steel framework," *Journal of Constructional Steel Research,* vol. 35, no. 3, pp. 377-408, 1995/01/01/ 1995, doi: https://doi.org/10.1016/0143-974X(95)00010-S.

[18] J. Ding and Y. C. Wang, "Temperatures in unprotected joints between steel beams and concrete-filled tubular columns in fire," *Fire Safety Journal,* vol. 44, no. 1, pp. 16-32, 2009/01/01/ 2009, doi: https://doi.org/10.1016/j.firesaf.2008.02.004.

[19] M. Malaska, M. Alanen, M. Salminen, T. Jokinen, and R. Ranua, "Fire Performance of Steel-Timber Hybrid Beam Section," *Fire Technology,* vol. 60, no. 4, pp. 2581-2600, 2024/07/01 2023, doi: https://doi.org/10.1007/s10694-023-01471-y.

[20] M. Fragiacomo, A. Menis, I. Clemente, G. Bochicchio, and A. Ceccotti, "Fire Resistance of Cross-Laminated Timber Panels Loaded Out of Plane," *Journal of Structural Engineering,* vol. 139, no. 12, p. 04013018, 2013/12/01 2013, doi: https://doi.org/10.1061/(ASCE)ST.1943-541X.0000787.

[21] J. C. Zhang, D. S. Zhang, Y. L. Dong, and W. H. Wang, "Experimental study on internal force variation of steel-concrete composite beam under fire," (in Chinese), *Engineering Mechanics,* vol. 36, no. 6, pp. 183-192,210, 2019, doi: https://doi.org/10.6052/j.issn.1000-4750.2018.05.0281.

[22] M. Godoy Dellepiani, G. Roa Munoz, S. J. Yanez, C. F. Guzmán, E. I. Saavedra Flores, and J. C. Pina, "Numerical study of the thermo-mechanical behavior of steel–timber structures exposed to fire," *Journal of Building Engineering,* vol. 65, p. 105758, 2023/04/15/ 2023, doi: https://doi.org/10.1016/j.jobe.2022.105758.

[23] E. Philion, B. Chorlton, J. Gales, and P. Kotsovinos, "Structural Fire Modeling Strategies for Exposed Mass Timber Compartments and Experimental Gaps for Model Validation," *Journal of Performance of Constructed Facilities,* vol. 36, no. 6, p. 04022049, 2022, doi: https://doi.org/10.1061/(ASCE)CF.1943-5509.0001761.

[24] S. H. Ingberg, "Tests of the Severity of Building Fires," NFPA Quarterly 22(1), pp. 43–61, 1928.

[25] T. Z. Harmathy, "The fire resistance test and its relation to real-world fires," *Fire and Materials,* vol. 5, no. 3, pp. 112–122, 1981.

[26] L. Bisby, J. Gales, and C. Maluk, "A contemporary review of large-scale non-standard structural fire testing," *Fire Science Reviews,* vol. 2, no. 1, p. 1, 2013/05/21 2013, doi: https://doi.org/10.1186/2193-0414-2-1.

[27] D. Lange, J. Sjöström, J. Schmid, D. Brandon, and J. Hidalgo, "A Comparison of the Conditions in a Fire Resistance Furnace When Testing Combustible and Non-combustible Construction," *Fire Technology,* vol. 56, no. 4, pp. 1621-1654, 2020/07/01 2020, doi: https://doi.org/10.1007/s10694-020-00946-6.

[28] W. Węgrzyński, P. Turkowski, and P. Roszkowski, "The discrepancies in energy balance in furnace testing, a bug or a feature?," *Fire and Materials,* vol. 2019, pp. 1-12, 08/08 2019, doi: https://doi.org/10.1002/fam.2735.

[29] P. H. Thomas and A. J. M. Heselden, *Fully-developed fires in single compartments: A co-operative research programme of the Conseil International du Bâtiment*. Borehamwood: Fire Research Station, 1972.

[30] O. Pettersson, S. E. Magnusson, and J. Thor, *Fire Engineering Design of Steel Structures*. Stockholm: Swedish Institute of Steel Construction, 1976.

[31] J. Stern-Gottfried and G. Rein, "Travelling fires for structural design-Part II: Design methodology," *Fire Safety Journal,* vol. 54, pp. 96-112, 2012/11/01/ 2012, doi: https://doi.org/10.1016/j.firesaf.2012.06.011.

[32] V. Gupta, "Open-plan compartment fire dynamics," PhD Thesis, School of Civil Engineering, The University of Queensland, 2021.

[33] BS EN 1993-1-2, *Eurocode 3: Design of steel structures - Part 1-2: General rules - Structural fire design*. British Standards Institution, 2005.

[34] BS EN 1992-1-2, *Eurocode 2: Design of concrete structures - Part 1-2: General rules - Structural fire design*. British Standards Institution, 2019.

[35] Z. Ma, J. Havula, and M. Heinisuo, "Structural fire analysis of simple steel structures by using LS-DYNA explicit solver," *Rakenteiden Mekaniikka,* vol. 52, pp. 1-22, 07/11 2019, doi: https://doi.org/10.23998/rm.77252.

[36] M. H. Nguyen, S.-E. Ouldboukhitine, S. Durif, V. Saulnier, and A. Bouchair, "Passive fire protection of steel profiles using wood," *Engineering Structures,* vol. 275, p. 115274, 2023/01/15/ 2023, doi: https://doi.org/10.1016/j.engstruct.2022.115274.

[37] M. H. Nguyen, S.-E. Ouldboukhitine, S. Durif, V. Saulnier, and A. Bouchair, "Method of measuring the temperature of wood exposed to fire with type K thermocouples," *Fire Safety Journal,* vol. 137, p. 103752, 2023/05/01/ 2023, doi: https://doi.org/10.1016/j.firesaf.2023.103752.

[38] V. D. Thi, M. Khelifa, M. Oudjene, M. E. Ganaoui, and Y. Rogaume, "Finite element analysis of heat transfer through timber elements exposed to fire," *Engineering Structures,* vol. 143, pp. 11-21, 2017/07/15/ 2017, doi: https://doi.org/10.1016/j.engstruct.2017.04.014.

[39] C. Chen, L. Jiang, J. Qiu, M. A. Orabi, W. Chan, and A. Usmani, "OpenSees development for modelling timber structural members subjected to realistic fire impact," *Fire and Materials,* 11/09 2022, doi: https://doi.org/10.1002/fam.3115.

[40] F.-X. Ding, W. Wang, and B. Jiang, "Numerical study on the fire behaviour of restrained steel-concrete composite beams," *Journal of Building Engineering,* vol. 70, p. 106358, 2023/07/01/ 2023, doi: https://doi.org/10.1016/j.jobe.2023.106358.

[41] A. I. Bartlett, R. M. Hadden, and L. A. Bisby, "A Review of Factors Affecting the Burning Behaviour of Wood for Application to Tall Timber Construction," *Fire Technology,* vol. 55, no. 1, pp. 1-49, 2019/01/01 2019, doi: https://doi.org/10.1007/s10694-018-0787-y.

[42] H. Xu *et al.*, "Large-scale compartment fires to develop a self-extinction design framework for mass timber—Part 1: Literature review and methodology," *Fire Safety Journal,* vol. 128, p. 103523, 2022/03/01/ 2022, doi: https://doi.org/10.1016/j.firesaf.2022.103523.

[43] I. Pope *et al.*, "Fully-developed compartment fire dynamics in large-scale mass timber compartments," *Fire Safety Journal,* vol. 141, p. 104022, 2023/12/01/ 2023, doi: https://doi.org/10.1016/j.firesaf.2023.104022.

[44] Arup Guide, "Fire Safe Design of Mass Timber Buildings," Arup, 2024.

[45] D. Hopkin *et al.*, "Large-Scale Enclosure Fire Experiments Adopting CLT Slabs with Different Types of Polyurethane Adhesives: Genesis and Preliminary Findings," *Fire,* vol. 5, no. 2, p. 39, 2022. [Online]. Available: https://www.mdpi.com/2571-6255/5/2/39.

[46] J.-C. Mindeguia, S. Mohaine, L. Bisby, F. Robert, R. McNamee, and A. Bartlett, "Thermo-mechanical behaviour of cross-laminated timber slabs under standard and natural fires," *Fire and Materials,* vol. 45, no. 7, pp. 866-884, 2020, doi: https://doi.org/10.1002/fam.2938.

[47] D. Brandon and C. Dagenais, "Fire Safety Challenges of Tall Wood Buildings – Phase 2: Task 5 – Experimental Study of Delamination of Cross Laminated Timber (CLT) in Fire," National Fire Protection Association, 2018.

[48] A. I. Bartlett, R. McNamee, F. Robert, and L. A. Bisby, "Comparative energy analysis from fire resistance tests on combustible versus noncombustible slabs," *Fire and Materials,* vol. 44, no. 3, pp. 301-310, 2020/04/01 2020, doi: https://doi.org/10.1002/fam.2760.

[49] L. M. R. Mesquita, P. A. G. Piloto, M. A. P. Vaz, and P. M. M. Vila Real, "Experimental and numerical research on the critical temperature of laterally unrestrained steel I beams," *Journal of Constructional Steel Research,* vol. 61, no. 10, pp. 1435-1446, 2005/10/01/ 2005, doi: https://doi.org/10.1016/j.jcsr.2005.04.003.

[50] M. Kucukler, "Lateral instability of steel beams in fire: Behaviour, numerical modelling and design," *Journal of Constructional Steel Research,* vol. 170, p. 106095, 2020/07/01/ 2020, doi: https://doi.org/10.1016/j.jcsr.2020.106095.

[51] A. D. Martins, D. Camotim, R. Gonçalves, N. Lopes, and P. Vila Real, "Transversally loaded stainless steel beams under fire: Local/global behaviour, strength and design," *Journal of Constructional Steel Research,* vol. 189, p. 107080, 2022/02/01/ 2022, doi: https://doi.org/10.1016/j.jcsr.2021.107080.

[52] T.-Y. Song, X.-Y. Qu, H. Zhou, and K. Xiang, "Advanced critical temperature method for steel beams exposed to different fire scenarios," *Structures,* vol. 44, pp. 200-215, 2022/10/01/ 2022, doi: https://doi.org/10.1016/j.istruc.2022.08.019.

[53] C. Zhang, G.-Q. Li, and A. Usmani, "Simulating the behavior of restrained steel beams to flame impingement from localized-fires," *Journal of Constructional Steel Research,* vol. 83, pp. 156-165, 2013/04/01/ 2013, doi: https://doi.org/10.1016/j.jcsr.2013.02.001.

[54] X. T. Nguyen and J. S. Park, "Design equations for buckling strength of steel I-beam under non-uniform heating condition," *Fire Safety Journal,* vol. 127, p. 103464, 2022/01/01/ 2022, doi: https://doi.org/10.1016/j.firesaf.2021.103464.

[55] M. Dwaikat and V. Kodur, "Engineering Approach for Predicting Fire Response of Restrained Steel Beams," *Journal of Engineering Mechanics,* vol. 137, pp. 447–461., 07/01 2011, doi: https://doi.org/10.1061/(ASCE)EM.1943-7889.0000244.

[56] BS EN 1994-1-2, *Eurocode 4: Design of composite steel and concrete structures - Part 1-2: General rules - Structural fire design*. British Standards Institution, 2005.

[57] CTICM, "Logiciel LTBeamN – Déversement élastique de poutres fléchies comprimées," 2023. [Online]. Available: https://www.cticm.com/logiciel/ltbeamn/.

[58] P. M. M. Vila Real, R. Cazeli, L. Simões da Silva, A. Santiago, and P. Piloto, "The effect of residual stresses in the lateral-torsional buckling of steel I-beams at elevated temperature," *Journal of Constructional Steel Research,* vol. 60, no. 3, pp. 783-793, 2004/03/01/ 2004, doi: https://doi.org/10.1016/S0143-974X(03)00143-3.

[59] Y. Z. Yin and Y. C. Wang, "Numerical simulations of the effects of non-uniform temperature distributions on lateral torsional buckling resistance of steel I-beams," *Journal of Constructional Steel Research,* vol. 59, no. 8, pp. 1009-1033, 2003/08/01/ 2003, doi: https://doi.org/10.1016/S0143-974X(03)00003-8.

[60] Y. Z. Yin and Y. C. Wang, "A numerical study of large deflection behaviour of restrained steel beams at elevated temperatures," *Journal of Constructional Steel Research,* vol. 60, no. 7, pp. 1029-1047, 2004/07/01/ 2004, doi: https://doi.org/10.1016/j.jcsr.2003.09.005.

[61] A. Santiago, L. S. da Silva, P. V. Real, and M. Veljkovic, "Numerical study of a steel sub-frame in fire," *Computers & Structures,* vol. 86, no. 15, pp. 1619-1632, 2008/08/01/ 2008, doi: https://doi.org/10.1016/j.compstruc.2008.01.006.

[62] C. Couto and P. Vila Real, "The influence of imperfections in the critical temperature of I-section steel members," *Journal of Constructional Steel Research,* vol. 179, p. 106540, 2021/04/01/ 2021, doi: https://doi.org/10.1016/j.jcsr.2021.106540.

[63] C. Couto and P. Vila Real, "Numerical investigation on the influence of imperfections in the lateral-torsional buckling of beams with slender I-shaped welded sections," *Thin-Walled Structures,* vol. 145, p. 106429, 2019/12/01/ 2019, doi: https://doi.org/10.1016/j.tws.2019.106429.

[64] STA, "Structural timber buildings fire safety in use guidance. Volume 6 - Mass timber structures; Building Regulation compliance B3(1)," Structural Timber Association, 2023.

[65] BS 476-20, *Fire tests on building materials and structures - Part 20: Method for determination of the fire resistance of elements of construction (general principles)*. British Standards Institution, 1987.